Northumbria
University
NEWCASTLE

ACS APPLIED MATERIALS & INTERFACES

www.acsami.org

Research Article

A Facile Surface Preservation Strategy for the Lithium Anode for High-Performance Li−O_2 Batteries

Zhihong Luo, Guangbin Zhu, Liankun Yin, Fujie Li, Ben Bin Xu, Laurent Dala, Xiaoteng Liu,* and Kun Luo*

Cite This: *ACS Appl. Mater. Interfaces* 2020, 12, 27316−27326

Read Online

ACCESS | Metrics & More | Article Recommendations | Supporting Information

ABSTRACT: Protecting an anode from deterioration during charging/discharging has been seen as one of the key strategies in achieving high-performance lithium (Li)−O_2 batteries and other Li−metal batteries with a high energy density. Here, we describe a facile approach to prevent the Li anode from dendritic growth and chemical corrosion by constructing a SiO_2/GO hybrid thin layer on the surface. The uniform pore-preserving layer can conduct Li ions in the stripping/plating process, leading to an effective alleviation of the dendritic growth of Li by guiding the ion flux through the microstructure. Such a preservation technique significantly enhances the cell performance by enabling the Li−O_2 cell to cycle up to 348 times at 1 A·g^{-1} with a capacity of 1000 mA·h·g^{-1}, which is several times the cycles of cells with pristine Li (58 cycles), Li−GO (166 cycles), and Li−SiO_2 (187 cycles). Moreover, the rate performance is improved, and the ultimate capacity of the cell is dramatically increased from 5400 to 25,200 mA·h·g^{-1}. This facile technology is robust and conforms to the Li surface, which demonstrates its potential applications in developing future high-performance and long lifespan Li batteries in a cost-effective fashion.

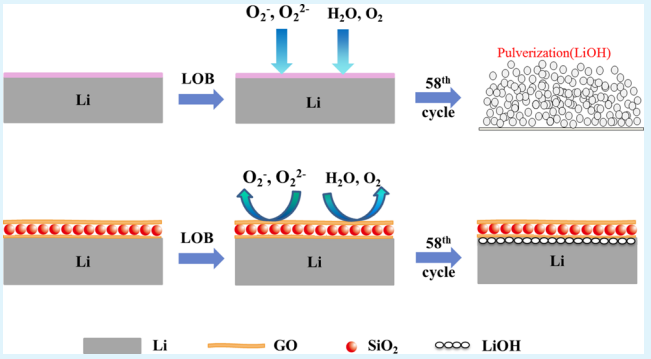

KEYWORDS: *lithium metal anode, SiO_2/GO coating, protective layer, cyclic stability, Li−O_2 battery*

INTRODUCTION

Aprotic Li−O_2 batteries (LOBs), a promising energy solution for automotive and aerospace engineering, have superior advantage because of their high energy densities, when compared with conventional lithium−/sodium−ion batteries (LIBs/SIBs).[1−8] Currently, the technical development in aprotic LOBs encounters substantial bottlenecks, including high charge overpotential, passivation of the cathode, and poor stability of the electrolyte and Li metal anode.[7] Significant efforts have been made to enhance the cyclic stability and other electrochemical performances of LOBs by promoting the sluggish kinetics of oxygen reduction and evolution using proper catalysts,[9] porous cathode materials,[10,11] redox mediators,[12,13] and stable electrolytes.[14,15]

Despite its natural scarcity, problematic stability, and safety issues,[7,8] Li metal is regarded as an ideal anode material for rechargeable batteries because of its superhigh specific energy (3860 mA·h·g^{-1}), low redox potential (−3.04 V vs standard hydrogen electrode), and low mass density (0.534 g·cm^{-3}). However, Li anodes encounter challenges such as the uneven stripping/plating of Li ions and the low Coulombic efficiency during charge/discharge cycles, which usually lead to the dendritic growth of Li to cause the short-circuiting and "dead Li" (i.e., broken Li branches) after the repeated charging/discharging operation[16] and a rapid degradation in the battery cell.[17] The decaying in LOBs can be accelerated as the crossover oxidative species such as soluble oxygen reduction intermediates (O_2^-, LiO_2^-, etc.), H_2O, and other reaction byproducts can accelerate Li loss, thus resulting in a declined cycle life.[18,19]

One of the recent research interests has been focused on the protection of Li anodes because the dendritic deposition of lithium metal and dendrite formation along the solid−electrolyte interphase (SEI) are unveiled as key issues to determine the safety and performance of LOBs.[20,21] The strategies exercised for protecting Li anodes can be categorized in the following: (1) using poreless, air-impermeable, and waterproof separators to prevent O_2, H_2O, and other soluble species in the electrolyte from corroding the anode in LOBs;[22−24] however, the increase of the overall cell resistance remains under concern. (2) Optimizing the structure of SEI layers, where the lifespans of LOBs can be extended after

Received: May 7, 2020
Accepted: May 21, 2020
Published: May 21, 2020

https://dx.doi.org/10.1021/acsami.0c08355
ACS Appl. Mater. Interfaces 2020, 12, 27316−27326

treating the SEI layers on Li anodes chemically (including the reaction with CO_2, N_2, and F- and B-containing electrolyte additives)[25−29] or electrochemically.[30−32] (3) Generating ionically conductive, mechanically robust, and chemically stable protection layer(s) on Li anodes, and the commonly used materials for such protection layers include polymers (e.g., poly(1,4-dioxacyclohexane)[33]), inorganic compounds (e.g., germanium or indium compounds[34−36]), and composites (e.g., Al_2O_3/PVDF-HFP or AlF_3/PEDOT-PEG[37,38]).

Graphene and graphene oxide (GO) have been reported previously to offer protection to the Li anode by preventing from dendrite growth, corrosion, and strengthening the stability of SEI.[39−43] Li and co-workers[39] employed reduced GO to prevent Li dendrites by directing their growth. Zhao et al.[41] encapsulated a Li alloy with graphene sheets to prevent the corrosion from air. Gao and co-workers[43] designed a molecular level SEI by embedding polymeric Li salts with GO, which provides the SEI to have excellent stability and good passivation properties, which prevents the Li metal anode from dendrite growth and corrosion. Silica was also used for Li metal protection. Tang and co-workers applied silica nanoparticles (SiO_2 NPs) in a cross-linked polymer solid-state electrolyte for increasing the Li ionic conductivity by forming 3D ion transport paths.[44] Lin et al. employed a silica aerogel as a backbone for a polymer electrolyte for high Li ionic conductivity and modulus.[45] Herein, we propose an anode protection strategy by developing an artificial composite layer consisting of SiO_2 NPs and GO nanosheets on the Li metal (Li−SiO_2/GO) anode. GO sheets act as a barrier to hinder the growth of Li dendrites and the deteriorative attack of oxygen species from the electrolyte; the SiO_2 NPs embedded in GO sheets can provide an effective interlayer and pores for Li ion diffusion by preventing the aggregation of GO sheets. With this designed protection, the LOBs with Li−SiO_2/GO anodes exhibit superior cycling stability, rate performance, and ultimate capacity. We hope this anode protection technology will find future applications in next-generation sustainable energy solutions.

EXPERIMENTAL SECTION

Chemicals and Materials. Potassium permanganate ($KMnO_4$, AR, Sinopharm Group), hydrogen peroxide (H_2O_2, 30%, Sinopharm Group), sodium nitrate ($NaNO_3$, AR, Sinopharm Group), and sulfuric acid (H_2SO_4, AR, Sinopharm Group) were used as received. Dimethyl ether (DME, anhydrous, 99.5%, Sigma-Aldrich), dimethyl sulfoxide (DMSO, 99.9%, Sigma-Aldrich), and propylene carbonate (PC, 99.7%, Sigma-Aldrich) were dehydrated with activated 4 Å molecular sieves. Lithium perchlorate ($LiClO_4$, 99.99%, Sigma-Aldrich) was dried at 160 °C in a vacuum oven for 12 h prior to use. Graphite (Sigma-Aldrich), silica NPs (SiO_2, $d = 30 \pm 5$ nm, Shanghai Keyan Co., Ltd.), multiwalled carbon nanotubes (MWNTs, $d = 10 \pm 1$ nm, $L = 3-6$ μm, Sigma-Aldrich), carbon paper (TORAY, TGPH-060), and borosilicate glass fiber (GF, $d = 18$ mm, Whatman) were used as received. Li plates ($d = 14$ mm, Shenzhen Poxon Machinery Technology Co. Ltd.) were saturated in a PC solution containing 0.1 M $LiClO_4$ for at least 48 h before use.

Preparation of SiO_2/GO Hybrids. GO was prepared using the modified Hummer's method.[46] Typically, 1.0 g of graphite, 0.5 g of $NaNO_3$, and 23 mL of H_2SO_4 were mixed and stirred at 0 °C for 1 h. The mixture was heated to 35 °C, and then 3.0 g of $KMnO_4$ was slowly added. After stirring for 7 h, another 3.0 g of $KMnO_4$ was added, and the mixture was kept stirring for the next 12 h. The mixture was cooled down in air, and then 400 mL of ice water was added under stirring. After that, 30 wt % H_2O_2 was gradually added until the color of the mixture turned from brown to yellow. The solid content in the mixture was separated by centrifugation at 8000 rpm and then repeatedly rinsed with deionized water until the supernatant became neutral. The precipitate was mixed with deionized water under ultrasonic stirring for 3 h and then allowed to stand for 12 h. The GO suspension in the container was removed and used for further synthesis.

SiO_2 NPs were ultrasonically dispersed in the GO suspension with a mass ratio of 1:2 (SiO_2/GO) for 2 h; the precipitate was then removed and dried in a vacuum oven at 80 °C for 24 h. The dried SiO_2/GO powder was carefully ground and then dispersed in DME (5 mg·mL^{-1}), where 0.5 mg of the slurry was repeatedly pipetted until it completely covered the surface of a Li plate, followed by a smoothening process using a fine blade, and after drying in a glove box at ambient temperature, the Li anode with protective SiO_2/GO coating is obtained and denoted Li−SiO_2/GO. The Li anodes coated with either monocomponent SiO_2 or GO were prepared as reference samples, denoted Li−SiO_2 and Li−GO, respectively. Various GO/SiO_2 mass ratios (0.5:1, 1:1, 2:1, 3:1, and 4:1) and loading amounts (0.1, 0.2, 0.6, 0.8, 1.0, and 1.5 mg) were prepared and constructed as a preserving layer on the Li anodes.

Battery Assembly and Testing. The batteries were assembled and built into CR2032 coin cells in an Ar-filled glove box (MIKROUNA, Super, $H_2O < 0.1$ ppm, $O_2 < 0.1$ ppm) and tested using a standard battery testing system (CT-3008W-5V10mA, Neware Technology Limited).

LOBs were assembled using both Li anodes and MWNT cathodes in the CR2032 cells. The Li anodes employed in the experiment included the pristine Li plate and Li plates with different surface coatings. The cathode was prepared by spraying the MWNTs in ethanol slurry onto a carbon paper at a loading of 0.1 mg·cm^{-2}. To assemble the coin cells, an anode cap was first placed, and then a Li anode (either pristine Li or one of the anodes with surface coatings), a glass fiber separator (wetted with 100 μL of 1 M $LiClO_4$/DMSO electrolyte), a MWNT cathode, and a cathode cap were placed in sequence and encapsulated. The cells were mounted separately in the holders of a home-made battery testing box filled with pure oxygen at 1.0 atm. The cyclic performance test was settled at a rate of 1 A·g^{-1} with a fixed capacity of 1000 mA·h·g^{-1} within the potential window from 2.0 to 4.5 V. The rate performance was measured at current densities of 2, 3, and 5 A·g^{-1}, and the capacity of 1000 mA·h·g^{-1} within the potential cutoff was from 2.0 to 4.5 V.

To characterize the ionic conductivity of coating layers, Li|SS (stainless steel) cells were assembled and subjected to electrochemical impedance spectroscopy (EIS) analysis in an O_2-free atmosphere. An anode cap, a Li plate, a GF separator (wetted with 100 μL of 1 M $LiClO_4$/DMSO electrolyte), a SS plate, and a CR2032 cathode cap (without holes) were placed in sequence and encapsulated to construct a Li|SS cell. To investigate the stability of Li anodes with surface coatings in an O_2 atmosphere, a Li|SS foam cell was assembled; the approach used was similar to the Li|SS cell, except for using a CR2032 cathode cap with holes and a SS foam to replace the SS plate. The Li|SS cells and Li|SS foam cells with Li−GO, Li−SiO_2, and Li−SiO_2/GO were also assembled using the same approaches. To characterize the resistance of LOBs (the assembly approach was the same as LOBs) after cycling for certain times, the EIS test was carried out after introducing N_2 to remove any O_2. All EIS plots were recorded on an electrochemical station (CHI 660, CH Instruments) at an open-circuit potential with 5 mV of ac amplitude in the frequency range from 0.1 Hz to 1 MHz.

Symmetric Li|Li cells were assembled to investigate the protection of Li anodes with different coatings in an O_2-free atmosphere, where an anode cap, a Li plate, a glass fiber separator (wetted with 100 μL of 1 M $LiClO_4$/DMSO electrolyte), another Li plate, and a CR2032 cathode cap (without holes) were placed in sequence and encapsulated. In the case of O_2, the Li plate with a hole (diameter of 2 mm) and a CR2032 cathode cap with holes were used, and the assembly approach was similar to those without O_2. The same approach was also applied to the assembly of symmetric Li|Li cells with Li−GO, Li−SiO_2, and Li−SiO_2/GO. The charge/discharge cycling was carried out with a time period fixed for 1 h at the current density of 0.1 mA·cm^{-2}.

Characterization. A field-emission scanning electron microscope (S-4800, Hitachi) and a transmission electron microscope (JEM-2100F) operating at 200 kV were employed to observe the morphology of the anodes and cathodes. An X-ray diffractometer (X'Pert PRO)

https://dx.doi.org/10.1021/acsami.0c08355
ACS Appl. Mater. Interfaces 2020, 12, 27316−27326

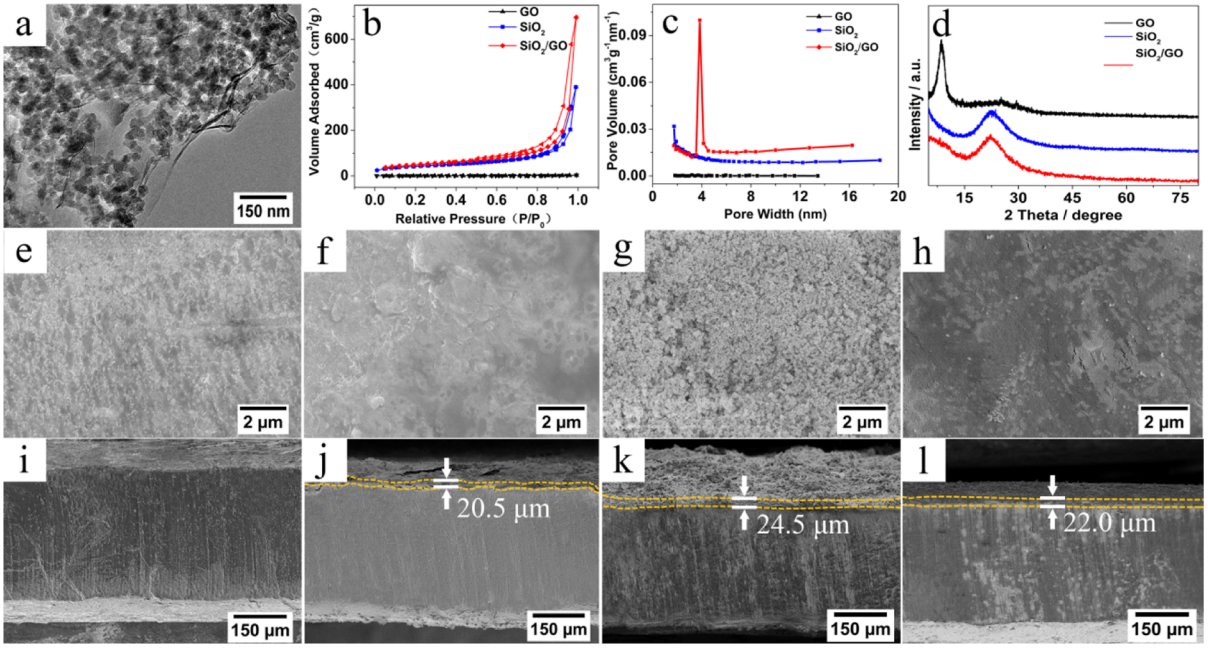

Figure 1. (a) TEM image of the SiO_2/GO hybrid; (b) N_2 adsorption/desorption isotherms; (c) pore distribution in the GO, SiO_2, and SiO_2/GO coatings; (d) XRD spectra of the GO, SiO_2, and SiO_2/GO coatings. Surface (e–h) and cross-sectional (i–l) images: (e,i) pristine Li, (f,j) Li–GO, (e,k) Li–SiO_2, and (h,l) Li–SiO_2/GO anodes.

equipped with a Cu Kα radiation source (λ = 1.54059 Å) was used to characterize the composition and structure of the coating and battery discharge products. An X-ray photoelectron spectrometer (ESCALAB 250Xi, Thermo Fisher Scientific) using Al Kα radiation was applied to characterize the components of coating layers and SEI. The electron conductivity of coating layers was measured using a high-temperature resistivity measurement system (RMS-1000I, Partulab Technologies). The specific surface area was determined from the N_2 adsorption/desorption isotherms using a surface area analyzer (NOVA1200e, Quantachrome).

RESULTS AND DISCUSSION

Structural Identification of Protective Coating Layers. Figure 1a reveals a laminated structure for the SiO_2/GO coating layer, that is, the SiO_2 NPs are intercalated among GO sheets, which effectively inhibits the overlapping aggregation of GO sheets and thereby produces nano-/mesopores for Li ion transportation. Two more cells with SiO_2 and GO individually coated anode were also assembled and tested for comparison; this is done to reveal the combined functions of both SiO_2 and GO when they are laminated together. Morphology information of SiO_2 and GO is shown in the TEM images in Figure S1.

The N_2 adsorption/desorption isotherms in Figure 1b demonstrate that both SiO_2 and SiO_2/GO exhibit type IV nitrogen sorption isotherms, while GO presents a low porosity likely because of the restacking of the GO sheets. The Brunauer–Emmett–Teller (BET) method shows that the SiO_2/GO coating delivers a specific surface area of up to 172.70 $m^2 \cdot g^{-1}$, SiO_2 presents a specific surface area of 146.25 $m^2 \cdot g^{-1}$, and the specific surface area of GO is just 2.35 $m^2 \cdot g^{-1}$. The estimated average pore sizes are 5.42 nm with a pore volume of 1.9×10^{-3} $cm^3 \cdot g^{-1}$ for the GO layer, 6.27 nm with a pore volume of 176×10^{-3} $cm^3 \cdot g^{-1}$ for the SiO_2 layer, and 3.8 nm with the largest pore volume of 312×10^{-3} $cm^3 \cdot g^{-1}$ for the SiO_2/GO layer (Figure 1c). The largest specific surface area of the SiO_2/GO coating layer is caused by the intercalation of SiO_2 NPs among the GO sheets, and this is in good agreement with the TEM results in Figure 1a.

Next, we used X-ray diffraction (XRD) analysis to assess the structure of the coating layers (Figure 1d). For the GO coating, an intense and sharp peak is observed at 8.8° corresponding to the interplanar spacing of ca. 1.0 nm of GO sheets,[47] and a bump at 25.2° resulted from the oxidized graphite. The XRD pattern of SiO_2 presents a broad peak at 22.6°, assigned to the (101) facet of silica (JCPDS no. 82-1235). As for the SiO_2/GO hybrid, a broad peak appears at about 22.6°, possibly attributed to the overlapped oxidized graphite and SiO_2 peaks, and the diffraction peak of GO at ca. 8.8° vanished, which indicates the absence of GO aggregation, in line with the TEM and BET analyses. We further applied X-ray photoelectron spectroscopy (XPS) to characterize the component of coating layers (Figure S2). The C_{1s} spectrum of the GO layer shows four peaks at 284.8, 286.5, 287.6, and 290.0 eV, which are assigned to the C–C, C–OH, C=O, and COOH groups, respectively (Figure S2a). The Si_{2p} spectrum of the SiO_2 layer displays one peak at 103.5 eV attributed to SiO_2 (Figure S2b). The C_{1s} and Si_{2p} spectra of the SiO_2/GO layer exhibit similar peaks, indicating that the SiO_2/GO composite contains the same component of GO and SiO_2 (Figure S2c,d).

SEM images of pure Li, Li–GO, Li–SiO_2, and Li–SiO_2/GO are shown in Figure 1e–l. For the pristine Li (Figure 1e), a flat and smooth surface is observed with a uniform SEI layer on top of the Li plate (Figure 1i). However, the SEM images of Li–GO (Figure 1f,j) and Li–SiO_2 (Figure 1g,k) indicate rough/smooth surfaces.[48] For the Li surface coated with the SiO_2/GO hybrid (Figure 1h,l), a smooth and compact surface layer was obtained, where the composite layer shows good adhesion with the Li surface. The protective layers are marked with an orange color dashed line, which are 20.5, 24.5, and 22.0 μm for the GO, SiO_2, and SiO_2/GO layers, respectively. The electron conductivity of GO, SiO_2, and SiO_2/GO composites is tested, which is 3.03 ×

https://dx.doi.org/10.1021/acsami.0c08355
ACS Appl. Mater. Interfaces 2020, 12, 27316–27326

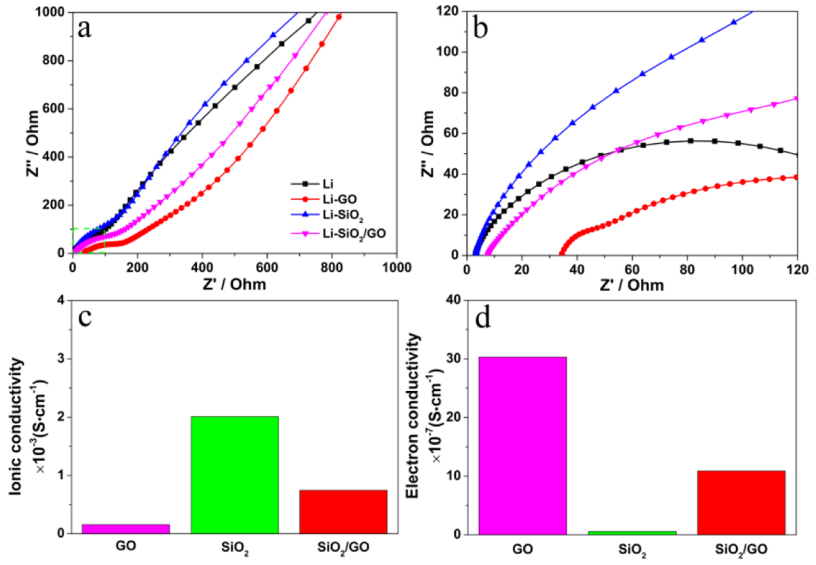

Figure 2. (a) Nyquist plots of the Li|SS cells with the pristine Li, Li−GO, Li−SiO_2, and Li−SiO_2/GO anodes; (b) the enlarged view of the green dotted frame; (c) ionic conductivity and (d) electron conductivity of GO, SiO_2, and SiO_2/GO coatings.

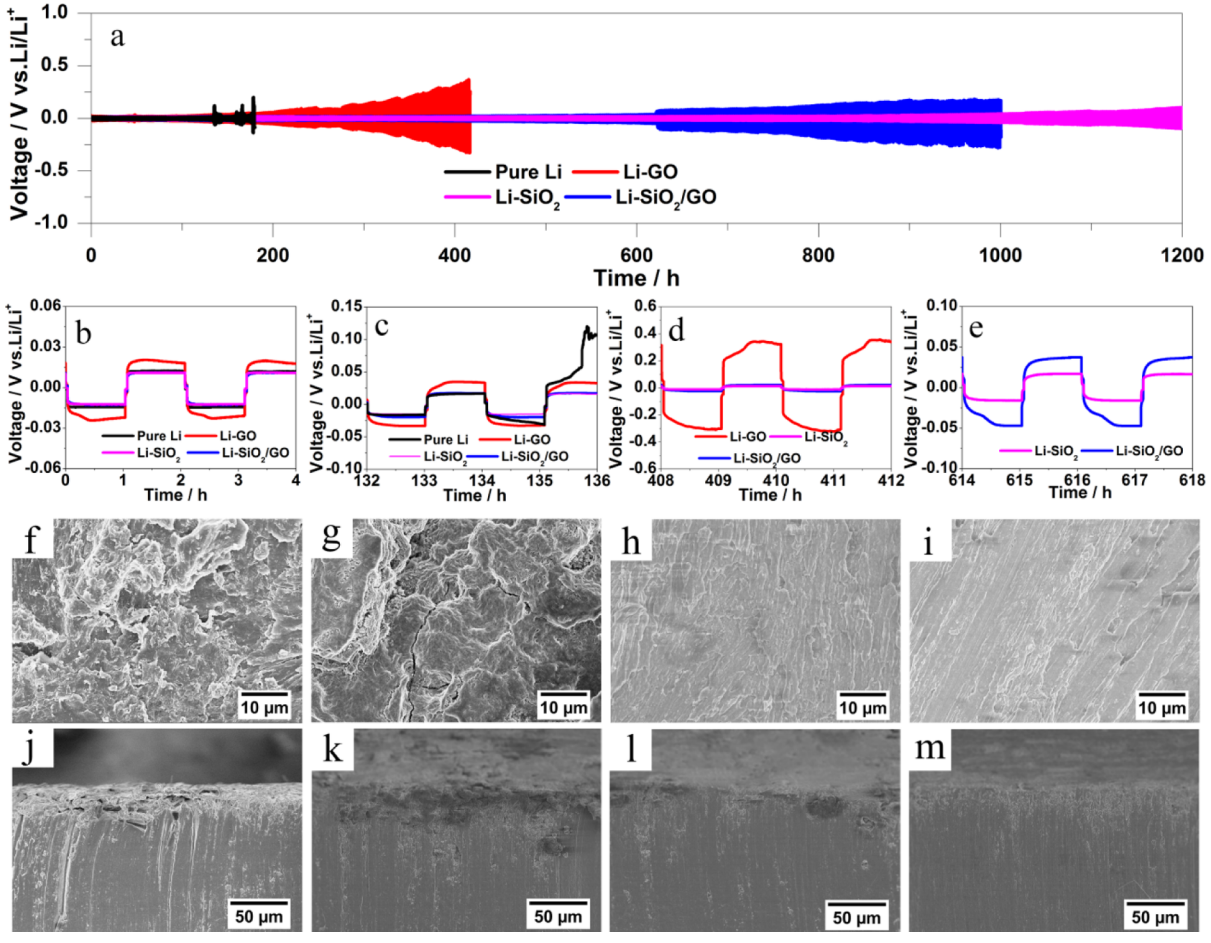

Figure 3. (a) Li stripping/plating curves in Li|Li symmetric cells with pristine Li, Li−GO, Li−SiO_2, and Li−SiO_2/GO at 0.1 mA·cm^{-2}. The selected voltage profiles are in the range from (b) 0 to 4, (c) 132 to 136, (d) 408 to 412, and (e) 614 to 618 h. Surface morphology and cross-sectional images of (f,j) Li, (g,k) Li−GO after 200 h, (h,l) Li−SiO_2, and (i,m) Li−SiO_2/GO after 800 h.

10^{-6}, 5.59 × 10^{-8}, and 1.09 × 10^{-6} S·cm^{-1} (Figure 2d), respectively.

The standard EIS analysis is used to compare the effect of GO, SiO_2, and SiO_2/GO coatings on the Li ion conductivity in Li|SS cells versus pristine Li, which is listed in Figure 2c.[38] The Nyquist plot (Figure 2a,b) shows that the intercept of the real axis represents the impedance of Li^+ diffusion (R_s) from the electrolyte solution to lithium metal.[38,49] In the cell with pristine

https://dx.doi.org/10.1021/acsami.0c08355
ACS Appl. Mater. Interfaces 2020, 12, 27316−27326

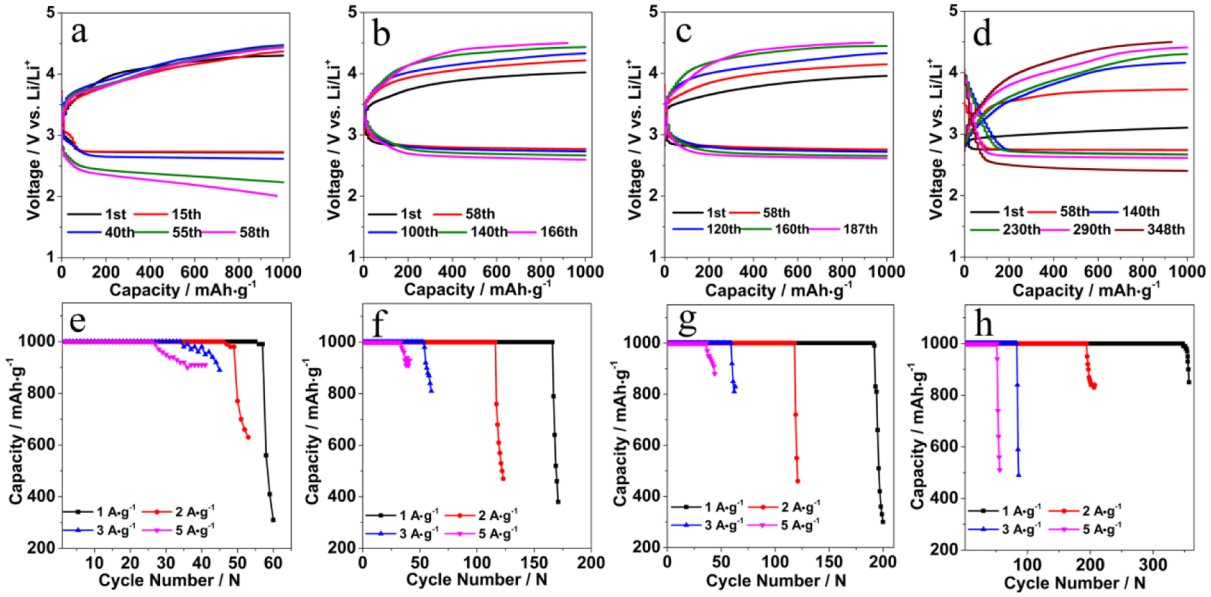

Figure 4. Cyclic stability (a–d) and rate performance (e–h) of the LOBs with (a,e) pristine Li, (b,f) Li–GO, (c,g) Li–SiO_2, and (d,h) Li–SiO_2/GO anodes.

Li, the impedance is 3.01 Ω. Compared to pristine Li, the impedance of the GO layer is 34.39 Ω, representing the Li ion conductivity of 1.56×10^{-4} S·cm^{-1}; this increase is due to the restacking of GO sheets that hinder the Li ion diffusion, in line with previous reports.[47,50] Li–SiO_2 delivers a comparable impedance of 3.21 Ω to pristine Li, which indicates the high Li ion conductance (2.01×10^{-3} S·cm^{-1}) within the SiO_2 NP layer. Li–SiO_2/GO exhibits a resistance of 7.76 Ω (conductivity of 7.46×10^{-4} S·cm^{-1}) for Li ion diffusion, which resulted from the high porosity of the hybrid layer that enhances the Li ion conductivity. EIS analysis of LilSS foam cells is conducted in an O_2 atmosphere to compare the stability of Li anodes with or without coating layers. As displayed in Figure S3a, the Nyquist plot of the pristine Li anode varied after staying in an O_2 atmosphere for 2 days; in contrast, with GO, SiO_2, and SiO_2/GO coatings (Figure S3b–d), the Nyquist plots of cells after 2 days showed a slight variation, implying that the stability of Li anodes with coating layers has improved.

Li Symmetric Battery Performance Evaluation. We carried out galvanostatic charge/discharge measurements to investigate the impact of surface coatings on the long-term cyclic stability of Li symmetric batteries with GO, SiO_2, and SiO_2/GO coating layers. The LilLi cells with a pair of pristine Li electrodes can only cycle for 134 h (Figure 3a), whereas a longer lifetime of 412 h is achieved after coating GO on the Li electrodes. The cycle life is further extended to 1200 and 1000 h, respectively, using the SiO_2 and SiO_2/GO coatings. The cycling performances of Li, Li–GO, Li–SiO_2, and Li–SiO_2/GO electrodes are compared within the initial 4 h (Figure 3b), where Li, Li–SiO_2, and Li–SiO_2/GO exhibit similar voltage profiles during the Li stripping/plating process at the magnitudes of about 26 mV. However, Li–GO presents a larger value of 48 mV, suggesting that a higher resistance was generated by the GO coating. From 132 to 136 h (Figure 3c), the voltage oscillation of Li–GO increased to ca. 70 mV, and the values of Li–SiO_2 and Li–SiO_2/GO electrodes remained unchanged. The pristine Li presents a sharp increase of overpotential after 135 h, suggesting a battery failure.[51] In Figure 3d, the voltage hysteresis of Li–GO is noticeably broadened over 600 mV between 408 and 412 h, indicating a battery failure; however, the amplitudes of Li–SiO_2 and Li–SiO_2/GO remained stable below 24 mV. After 614 h (Figure 3e), the potential oscillation of Li–SiO_2/GO (88 mV) becomes larger than Li–SiO_2 (34 mV) and keeps increasing to 475 mV until the battery fails at 1000 h. Li–SiO_2 manifests the longest cycling life and ends up at 1200 h.

The morphology of Li metals during cycling was characterized and is shown in Figure 3f–m. After 200 h of operation, Li metal of the LilLi cell exhibits a coarse surface topped with mossy Li (Figure 3f, top-view SEM image), and the side-view SEM image shows that large cracks appeared on the top layer, with several cracks showing a clear tendency to reach deeper layers (Figure 3j). With only GO coating, as seen from the top-view image (Figure 3g), cracks caused by mossy Li are still observed on the surface of the Li metal; however, cracks are hardly seen on the side-view image (Figure 3k). Figure 3j,k shows a fluffy profile on the top layer mossy Li, which looks different from the pure Li metal; this is the evidence that the surface of these two anodes has been corroded. Those cells with SiO_2 (Figure 3h,l) and SiO_2/GO (Figure 3i,m) coating layers have no obvious mossy Li, and cracks can be seen after cycling for 800 h; in addition, the cross-sectional image shows a compacted SEI. These results demonstrate that SiO_2 and SiO_2/GO coating layers can facilitate stable SEI formation and regulate Li deposition.

The long-term cyclic stability of Li symmetric batteries with GO, SiO_2, and SiO_2/GO coating layers was also investigated in an O_2 atmosphere. As shown in Figure S4a, the LilLi cells with a pristine Li electrode can only cycle for 80 h; in contrast, the cells with GO, SiO_2, and SiO_2/GO layers can cycle up to 250, 300, and 480 h, respectively. During the first 4 h (Figure S4b), LilLi cells with pristine Li, Li–SiO_2, and Li–SiO_2/GO present a discharge overpotential of 8 mV, but it is 34 mV for the Li–GO electrode. In the charge process, LilLi cells with pristine Li, Li–GO, and Li–SiO_2 show an overpotential of 36 mV, and it is 16 mV for the Li–SiO_2/GO electrode. The LilLi cell with the Li–SiO_2/GO electrode also exhibits the smallest overpotential during the discharge and charge processes. This could be due to the SiO_2/GO layer that formed the most stable SEI on the Li surface. From 80 to 84 h (Figure S4c), the LilLi cell with pristine

https://dx.doi.org/10.1021/acsami.0c08355
ACS Appl. Mater. Interfaces 2020, 12, 27316–27326

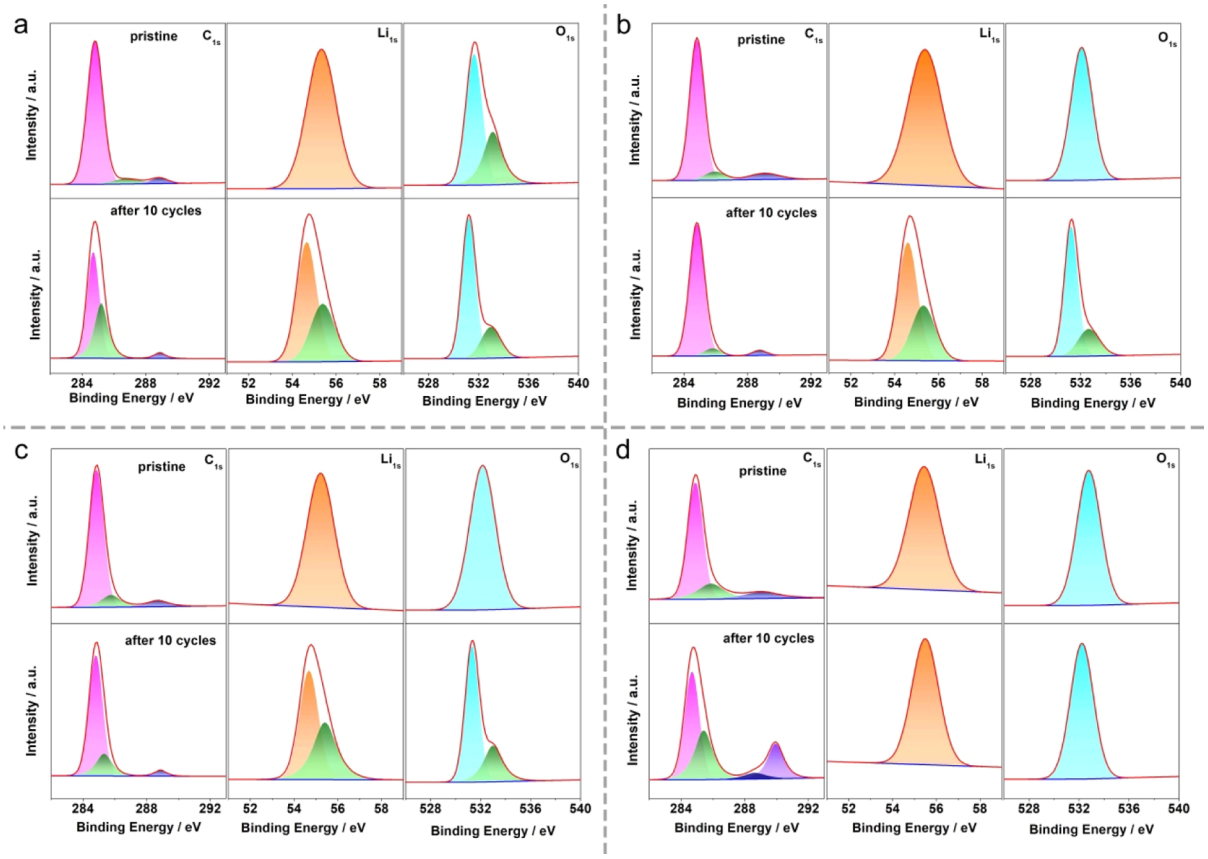

Figure 5. C_{1s}, Li_{1s}, and O_{1s} spectra of SEI components of the pristine Li anode (top) and after 10 cycles (bottom): (a) Li anode, (b) Li−GO anode, (c) Li−SiO_2 anode, and (d) Li−SiO_2/GO anode.

Li shows severe potential oscillation, which is an indication of the cell failure. However, LilLi cells with the Li−SiO_2 and Li−SiO_2/GO electrode showed an overpotential of 44 mV, but the Li−GO electrode showed 72 mV. After 250 h (Figure S4d), the overpotential of LilLi cells with Li−GO Li−SiO_2 electrodes increased by 2 V and 700 mV, respectively, but the increase is only about 100 mV for the cell with the Li−SiO_2/GO electrode. After 300 h (Figure S4e), the increase in the overpotential of Lil Li cells with the Li−SiO_2 electrode is more than 2 V, but it is only 140 mV for the one with the Li−SiO_2/GO electrode. Although the overpotential increases during the Li stripping/plating process in the O_2 atmosphere, the cell with the Li−SiO_2/GO electrode still maintains the lowest overpotential, implying that the SiO_2/GO layer improves the stability of the Li anode.

The morphology of Li electrodes from LilLi cell cycling in the O_2 atmosphere can be found in Figure S4f−m. After cycling for 80 h, the Li electrode generated a lot of powder on the surface (Figure S4f); large cracks and a thick layer of powder can be observed from the side view (Figure S4j); this white powder is the corrosion product of LiOH. Morphology of Li−GO, Li−SiO_2, and Li−SiO_2/GO electrodes after operating for 200 h is also characterized. Compared to the Li electrode, Li−GO and Li−SiO_2 anodes produced less powder on the surface (Figure S4g,h), and no obvious cracks are visible from the side view (Figure S4k,l). The Li−SiO_2/GO electrode shows an appearance with a smoother surface and a better evenly distributed cross section (Figure S4i,m).

LOB Performance Evaluation. The cyclic stability and rate performance of LOBs with the pristine Li, Li−GO, Li−SiO_2, and Li−SiO_2/GO anodes are assessed and compared (Figure 4). The cell with pristine Li can only operate for 58 cycles (Figure 4a). The discharge potential stays at about 2.72 V before the 15th cycle and then gradually dropped to 2.22 V at the 58th cycle. The charge potential keeps increasing from 4.10 V from the 1st cycle and ends up with ca. 4.24 V at the 58th cycle. The charge/discharge profiles of the cell with the Li−GO anode in Figure 4b suggest a better cyclic performance 166 times. The discharge plateau is maintained at 2.79 V within the initial 58 cycles, which then reduced down to 2.63 V at the 166th cycle. The charge plateau starts from 3.90 V at the 1st cycle and gradually increases to 4.42 V at the 166th cycle. The cell with the Li−SiO_2 anode can cycle 187 times, as displayed in Figure 4c, during which the discharge voltage is maintained at 2.76 V within 120 cycles and finally decreases to 2.64 V at the 187th cycle. The charge voltage is located at 3.83 V at the 1st cycle and approaches 4.41 V at the end.

Interestingly, the Li−SiO_2/GO anode (Figure 4d) presents the best battery performance with a significantly extended lifespan of the LOB cell to 348 cycles. The discharge voltage remains above 2.70 V for 230 cycles and then declines to 2.43 V at the 348th cycle. The charge voltage begins with just 3.03 V at the 1st cycle, which increases to 3.68 V at the 58th cycle, 3.98 V at the 230th cycle, 4.12 V at the 290th cycle, and finishes as 4.30 V at the 348th cycle. The LOB with the Li−SiO_2/GO anode also renders a better rate performance than the others (Figure 4e−h). At the rate of 2 $A \cdot g^{-1}$, the cell with the Li−SiO_2/GO anode can operate 194 times, higher than the cells with the pristine Li (46 times), Li−GO (116 times), and Li−SiO_2 anodes (118 times). At the rate of 3 A g^{-1}, the cells with the pristine Li, Li−GO, and Li−SiO_2 anodes can run for 34, 53, and 59 cycles, and

https://dx.doi.org/10.1021/acsami.0c08355
ACS Appl. Mater. Interfaces 2020, 12, 27316−27326

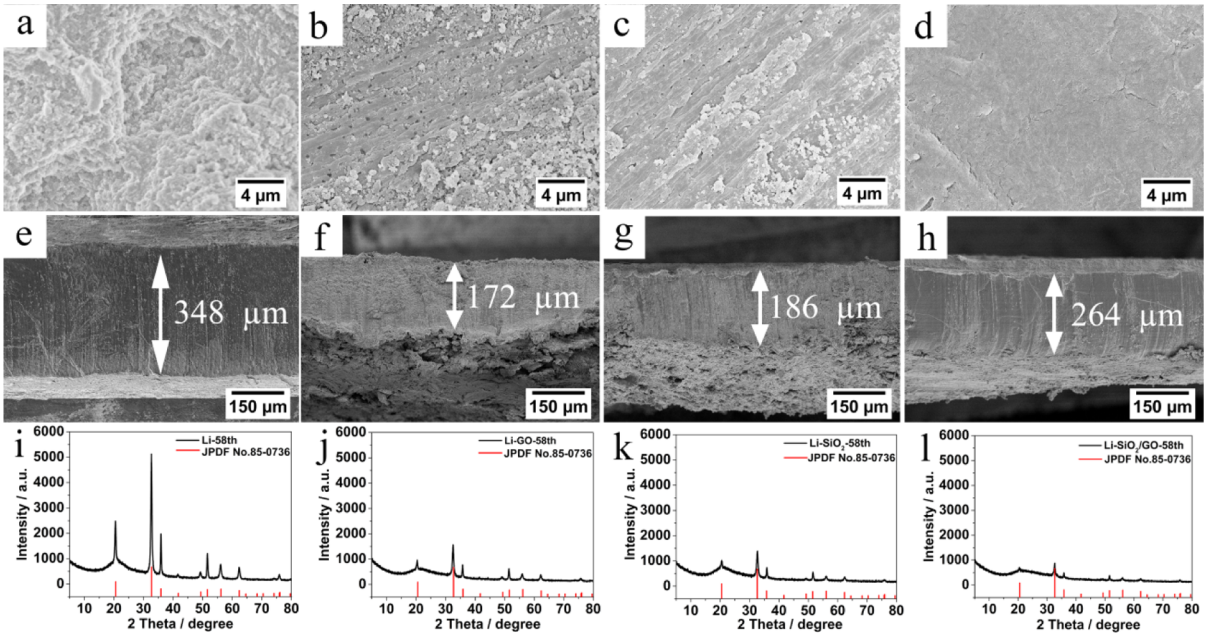

Figure 6. Surface of the Li anode at the 58th cycle: (a) pristine Li, (b) Li−GO anode, (c) Li−SiO_2 anode, and (d) Li−SiO_2/GO anode; cross section of the (e) pristine Li and Li anodes at the 58th cycle: (f) Li−GO anode, (g) Li−SiO_2 anode, and (h) Li−SiO_2/GO anode; XRD patterns of the Li anode at the 58th cycle: (i) pristine Li anode, (j) Li−GO anode, (k) Li−SiO_2 anode, and (l) Li−SiO_2/GO anode.

the cell with the Li−SiO_2/GO anode can run 83 times. At 5 A·g^{-1}, the cells with the pristine Li, Li−GO, and Li−SiO_2 anodes can cycle 26, 33, and 36 times, and the cell with the Li−SiO_2/GO anode can operate 56 times. Moreover, an ultimate capacity of the LOB with the Li−SiO_2/GO anode is achieved at 25,200 mA·h·g^{-1} (Figure S5), while the cells with pristine Li, Li−GO, and Li−SiO_2 anodes show values as 5400, 19,900, and 23,700 mA·h·g^{-1}, respectively.

The LOB performance can be affected by the SiO_2/GO mass ratio and loading amount. As shown in Figure S6a, the cycle numbers of the Li anodes with SiO_2/GO coatings are larger than those with sole GO or SiO_2 coating; the best performance appears at the SiO_2/GO mass ratio of 1/2. In Figure S6b, we obtain the cycle numbers of 160, 180, 348, 215, 192, 176, and 159 for the Li−SiO_2/GO anodes with a SiO_2/GO weight of 0.1, 0.2, 0.5, 0.6, 0.8, 1.0, and 1.5 mg, respectively, with the SiO_2/GO mass ratio of 1/2. An optimized loading is determined to be 0.5 mg of the coating materials applied on the Li anode. The TEM images of SiO_2/GO with different mass ratios demonstrate that SiO_2 NPs severely aggregate when the GO/SiO_2 ratio is 0.5/1 (Figure S7a) and 1/1 (Figure S7b), and no SiO_2 NPs filling in some areas of GO layers and multilayered covering of GO are also observed when the GO/SiO_2 ratio is 3/1(Figure S7c) and 4/1(Figure S7d). The side-view SEM images of Li−SiO_2/GO with different loading amounts (Figure S8) reveal a smooth and compact morphology for the SiO_2/GO layers when the loading amount is less than 0.6 mg, and a rough and cracked morphology when the loading mass exceeds 1.0 mg, which is in agreement with the above battery testing results.

Structural Examination and Failure Analysis for Variant Li Anodes after Cycling. SEI evolution of Li anodes is investigated by XPS (Figure 5, Table S1). For the pristine Li anode (Figure 5a, top 3 spectra), the C_{1s} spectrum shows three peaks at 284.8, 286.8, and 288.8 eV; the Li_{1s} spectrum exhibits a peak at 55.4 eV; and the O_{1s} spectrum displays two peaks at 531.7 eV and 533.1 eV; these indicate the existence of RCOCOOLi after soaking in the PC electrolyte for 48 h. As for Li−GO (Figure 5b, top 3 spectra), Li−SiO_2 (Figure 5c, top 3 spectra), and Li−SiO_2/GO anodes (Figure 5d, top 3 spectra), C_{1s} spectra exhibit three peaks at 284.8, 285.5, and 288.8 eV; Li_{1s} shows a peak at 55.4 eV; and O_{1s} shows a peak at 532.6 eV, attributing to RCH_2COOLi. The discrepancies between the Li anodes with or without coating layers are possibly because Li plates with coating layers are not pretreated with the PC electrolyte, and DME used as a dispersant for GO and SiO_2 composites contributed to the formation of RCH_2COOLi. After cycling 10 times, the C_{1s} spectra of Li (Figure 5a, bottom 3 spectra), Li−GO (Figure 5b, bottom 3 spectra), and Li−SiO_2 (Figure 5c, bottom 3 spectra) anodes show three peaks at 284.8, 285.5, and 288.8 eV; Li_{1s} spectra display two peaks at 54.6 and 55.4 eV; and O_{1s} spectra exhibit two peaks at 531.2 and 532.6; Li_{1s} of 54.6 eV and O_{1s} of 531.2 eV belong to LiOH, indicating that the corrosion occurs in the Li anode. In contrast, for the Li−SiO_2/GO anode (Figure 5d, bottom), the C_{1s} spectrum shows four peaks at 284.8, 285.4, 288.8, and 289.9 eV; Li_{1s} and O_{1s} exhibit one peak at 55.4 and 532.6 eV, respectively. C_{1s} of 289.9 eV is assigned to Li_2CO_3, possibly because the oxygen groups of GO participate in the formation of SEI. These results imply that after 10 cycles, RCOOLi and Li_2CO_3 are the main components of the SEI, and corrosion of the Li−SiO_2/GO anode by H_2O is inhibited by the SiO_2/GO coating layer.

Morphological evolution after charge/discharge cycling reveals the role of surface coating in preserving the Li anode. Figure 6a show the pristine Li anode and the pulverized anode after 58 cycles, which originally possesses a thickness of 348 μm (Figure 6e), suggesting that the battery failure is associated with the fast consumption of Li. The Li−GO anode presents a rough surface at the 58th cycle (Figure 6b), where Li metal still retains a thickness of 172 μm (Figure 6f). The Li−SiO_2 anode also shows a coarsened and scraggy surface after cycling 58 times (Figure 6c), leaving the Li metal with a thickness of about 186 μm (Figure 6g). As for the Li−SiO_2/GO anode, a smooth and compact surface is retained after 58 cycles (Figure 6d) with the average thickness of metallic Li for up to 264 μm (Figure 6h),

https://dx.doi.org/10.1021/acsami.0c08355
ACS Appl. Mater. Interfaces 2020, 12, 27316−27326

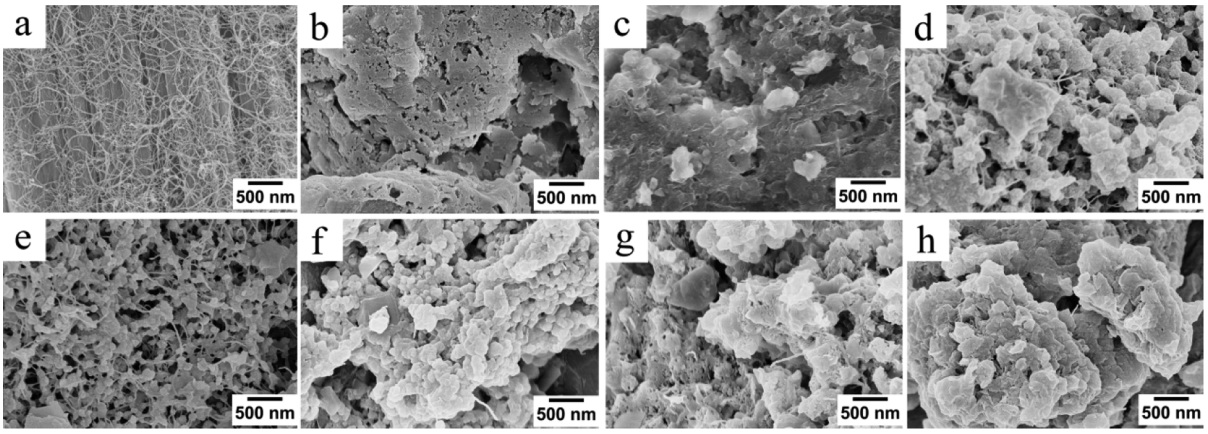

Figure 7. SEM images of the (a) pristine MWNT cathode and (b) MWNT cathode in the LOBs with the Li anode at the 58th cycle, (c,f) Li−GO anode at the 58th and 166th cycles, (d,g) Li−SiO_2 anode at the 58th and 187th cycles, and (e,h) Li−SiO_2/GO anode at the 58th and 348th cycles.

which offers a solid evidence to show the effective protection offered by the SiO_2/GO hybrid coating. Figure 6i−l displays the XRD patterns of powder from Li, Li−GO, Li−SiO_2, and Li−SiO_2/GO anodes' surface after 58 cycles. The powders from the pristine Li anode manifest 11 peaks at 20.4, 32.5, 35.7, 41.6, 49.2, 51.4, 56.0, 62.2, 73.9, 75.7, and 79.4°, which can be assigned to the (001), (101), (110), (002), (102), (200), (112), (211), (212), (220), and (221) facets of the LiOH crystal (JCPDS no. 85-0736). The intensity decreases in the order of pristine Li, Li−GO, Li−SiO_2, and Li−SiO_2/GO anodes, indicating the decreased amount of LiOH, in line with the increasing thickness of the Li anode after 58 cycles (Figure 6f−h). This further proved that the corrosion of the Li anode has been alleviated by the protective coating. The SEM images and XRD patterns of Li−GO anodes after 166 cycles (Figure S9a,d), of Li−SiO_2 anodes after 187 cycles (Figure S9b,e), and of Li−SiO_2/GO anodes after 348 cycles (Figure S9c,f) exhibit the same feature as the pristine Li anode, which show the identical products at battery failure.

It has been reported that highly active cross-over oxygen reduction intermediates (O_2^- and LiO_2^-) attack the Li anode and cause corrosion; they also react with the electrolyte and produce water molecules which are harmful to the Li metal.[15,18,23,31] Sun et al. revealed that the side reaction and the volume evolution of the Li anode also caused damage to the cathode using neutron tomography.[52] Our previous work indicates that the protection of the Li anode by creating a stable SEI can also alleviate the passivation of the cathode.[31] Here, Figure 7 shows that when the Li anode is protected with an artificial layer, such as GO, SiO_2, and SiO_2/GO, the accumulation of solid products on the cathode is reduced.

Accumulation of solid discharge products can result in the passivation of the MWNT cathode, thus leading to battery failure, which can be traced from the SEM image of the pristine MWNT cathode in Figure 7a. For the cell with a pristine Li anode (Figure 7b), the MWNT cathode is totally covered with large blocks of discharge products at the 58th cycle, representing the passivation of the battery cathode. As for the cells with Li−GO (Figure 7c), Li−SiO_2 (Figure 7d), and Li−SiO_2/GO (Figure 7e) anodes, bare MWNTs can still be observed after 58 cycles, where the amount and particle size of the deposit in the cell with the Li−SiO_2/GO anode are apparently less than the others. The MWNT cathodes are finally cladded by large deposit blocks for cells with the Li−GO (Figure 7f), Li−SiO_2 (Figure 7g), and Li−SiO_2/GO (Figure 7h) anodes after 166, 187, and 348 cycles, respectively, illustrating the alleviation of discharge product accumulation with the application of protective coatings on the Li anodes.

XRD analysis indicates that the MWNT cathode in the cell with the pristine Li anode after 58 cycles manifests two peaks at 26.4 and 54.5°, corresponding to the (002) and (004) facets of MWNTs (JCPDS no. 41-1487), as shown in Figure S10a, and the peak at 32.5° can be attributed to the (101) facet of the LiOH crystal (JCPDS no. 85-0736). Correspondingly, the MWNT cathode in the cell with the Li−SiO_2/GO anode also presents one peak at 32.5°, which is attributed to the (101) facet of LiOH (JCPDS no. 85-0736) at the 58th cycle (Figure S10b), and the intensity is much lower than that of the cell with pure Li, indicating that less solid products are accumulated, which is confirmed by the SEM image of the cathode (Figure 7e). At the 348th cycle (Figure S10c), the intensity of the three identifying peaks (at 20.4, 35.7, and 51.4° attributed to the (001), (110), and (200) facets of LiOH) increased; the process is much slower than that of the MWNT cathode from the cell with pristine Li. The presence of LiOH on both the cathode and the anode indicates the irreversible consumption of Li. The application of a coating layer effectively reduces the Li loss that normally arose from the dendritic growth, volume change, and corrosion during the stripping/plating process, which subsequently reduces the polarization and alleviates the cathode passivation.

Further investigation using electrochemical impedance proves the protection effect of the artificial layer. After cycling 58 times, N_2 was introduced into LOBs to remove O_2 for 30 min, and then the resistance of LOBs was characterized by EIS. Figure S11 presents the Nyquist plots of the LOBs with pristine Li, Li−GO, Li−SiO_2, and Li−SiO_2/GO as anodes and the equivalent circuit. Solution resistance (R_s), constant phase element 1 (CPE_1), and charge-transfer resistance (R_1) at the high-frequency region are assigned to the impedance at the Li/electrolyte interface; the constant phase element (CPE_2) and charge-transfer resistance (R_2) at the medium frequency region contributed to the impedance at the solid product/cathode interface. Values of resistance are shown in Table S2. The R_s, R_1, and R_2 of LOBs with pure Li are 219.0, 248.5, and 329.0 Ω, respectively. Those values of the cell anode coated with GO and SiO_2 layers are reduced to 48.4, 83.4, and 93.4 Ω, and to 41.4, 69.3, and 86.4 Ω, respectively. The values are further reduced to 34.2, 17.8, and 74.1 Ω with the Li−SiO_2/GO-coated anode. In agreement with morphology observation in Figures 6 and 7, EIS results

https://dx.doi.org/10.1021/acsami.0c08355
ACS Appl. Mater. Interfaces 2020, 12, 27316−27326

confirmed that the protection coatings led to a more stable Li anode and a less passivated cathode.

We considered that the nano-/mesopores introduced by SiO_2 NPs in the coating layer not only facilitate the diffusion of Li ions but also act as a guide for the uniform Li ion flux in the stripping/plating process, which reduces the risk of localized Li dissolution and suppresses the dendritic growth of Li.[53−58] In practical LOBs, the introduction of the oxygen reduction reaction brings soluble intermediates (such as O_2^- and LiO_2^-) and the decomposed byproducts of the electrolyte.[40,58] These may immigrate through the GF separator and cause serious chemical corrosion of Li anodes. Here, the incorporation of SiO_2 and GO manifests a synergistic effect of the barrier effect, the ionic conductance, and the Li ion flux guidance. The SiO_2/GO layer in this research provides the best protection for the Li anode, leading to the most stable LOB that has never been reported elsewhere.

CONCLUSIONS

In summary, we describe a facile strategy to preserve the Li anode by coating a SiO_2/GO composite layer, so that the dendritic growth and chemical corrosion of the Li anode during the electrochemical activities can be largely minimized or prevented. The structural composite layer with a large amount of nanopores resulted from the intercalation of SiO_2 NPs among the GO sheets, yielding an enhanced transportation of Li ions. The resultant LOB with the Li−SiO_2/GO anode can reach more than 348 cycles at 1 $A{\cdot}g^{-1}$ with a capacity of 1000 $mA{\cdot}h{\cdot}g^{-1}$, which is several times the cells with the pristine Li (58 cycles), Li−GO (166 cycles), and Li−SiO_2 (187 cycles) anodes. The rate performance and ultimate capacity of the LOB with the Li−SiO_2/GO anode are also significantly improved. We hope that this low-cost coating strategy find applications in future LIB technologies.

ASSOCIATED CONTENT

Supporting Information

The Supporting Information is available free of charge at https://pubs.acs.org/doi/10.1021/acsami.0c08355.

TEM images, ultimate capacity curves of LOBs, cyclic performance comparison of LOBs, SEM images, XRD patterns, Nyquist plots, XPS investigation of SEI evolution of LOBs, and EIS analysis of LOBs (PDF)

AUTHOR INFORMATION

Corresponding Authors

Xiaoteng Liu − *Department of Mechanical & Construction Engineering, Faculty of Engineering and Environment, Northumbria University, Newcastle upon Tyne NE1 8ST, U.K.*; orcid.org/0000-0001-7574-1709; Email: terence.liu@northumbria.ac.uk

Kun Luo − *School of Materials Science and Engineering, Changzhou University, Changzhou 213164, P. R. China; College of Materials Science and Engineering, Guilin University of Technology, Guilin 541004, P. R. China*; orcid.org/0000-0001-6526-4304; Email: luokun@cczu.edu.cn

Authors

Zhihong Luo − *College of Materials Science and Engineering, Guilin University of Technology, Guilin 541004, P. R. China*

Guangbin Zhu − *College of Materials Science and Engineering, Guilin University of Technology, Guilin 541004, P. R. China*

Liankun Yin − *College of Materials Science and Engineering, Guilin University of Technology, Guilin 541004, P. R. China*

Fujie Li − *College of Materials Science and Engineering, Guilin University of Technology, Guilin 541004, P. R. China*

Ben Bin Xu − *Department of Mechanical & Construction Engineering, Faculty of Engineering and Environment, Northumbria University, Newcastle upon Tyne NE1 8ST, U.K.*; orcid.org/0000-0002-6747-2016

Laurent Dala − *Department of Mechanical & Construction Engineering, Faculty of Engineering and Environment, Northumbria University, Newcastle upon Tyne NE1 8ST, U.K.*

Complete contact information is available at: https://pubs.acs.org/10.1021/acsami.0c08355

Author Contributions

Z.L. and G.Z. contributed equally. The manuscript was written through contributions of all authors. All authors have given approval to the final version of the manuscript.

Notes

The authors declare no competing financial interest.

ACKNOWLEDGMENTS

This work was supported by the National Natural Science Foundation of China (grant no. 51874051), the UK Engineering Physics and Science Research Council (grant no. EP/S032886/1), and the Natural Science Foundation of Guangxi (grant nos. 2018GXNSFAA281184 and 2019GXNSFAA245046).

REFERENCES

(1) Feng, N.; He, P.; Zhou, H. Critical Challenges in Rechargeable Aprotic Li-O_2 Batteries. *Adv. Energy Mater.* **2016**, *6*, 1502303.

(2) Yuan, T.; Jiang, Y.; Sun, W.; Xiang, B.; Li, Y.; Yan, M.; Xu, B.; Dou, S. Ever-Increasing Pseudocapacitance in RGO-MnO-RGO Sandwich Nanostructures for Ultrahigh-Rate Lithium Storage. *Adv. Funct. Mater.* **2016**, *26*, 2198−2206.

(3) Jiang, Y.; Li, Y.; Sun, W.; Huang, W.; Liu, J.; Xu, B.; Jin, C.; Ma, T.; Wu, C.; Yan, M. Spatially-confined lithiation-delithiation in highly dense nanocomposite anodes towards advanced lithium-ion batteries. *Energy Environ. Sci.* **2015**, *8*, 1471−1479.

(4) Kong, L.; Liu, X.; Wei, J.; Wang, S.; Xu, B. B.; Long, D.; Chen, F. T-Nb_2O_5 Nanoparticle Enabled Pseudocapacitance with a Fast Li-Ion Intercalation. *Nanoscale* **2018**, *10*, 14165−14170.

(5) Jiang, Y.; Hu, M.; Zhang, D.; Yuan, T.; Sun, W.; Xu, B.; Yan, M. Transition Metal Oxides for High Performance Sodium Ion Battery Anodes. *Nano Energy* **2014**, *5*, 60−66.

(6) Yu, S.; Li, Y.; Lu, Y.; Xu, B.; Wang, Q.; Yan, M.; Jiang, Y. A Promising Cathode Material of Sodium Iron-Nickel Hexacyanoferrate for Sodium Ion Batteries. *J. Power Sources* **2015**, *275*, 45−49.

(7) Ma, S.; Zhang, Y.; Cui, Q.; Zhao, J.; Peng, Z. Understanding Oxygen Reactions in Aprotic Li-O_2 Batteries. *Chin. Phys. B* **2016**, *25*, 018204.

(8) Guo, J.; Zhao, S.; Yang, H.; Zhang, F.; Liu, J. Electron Regulation Enabled Selective Lithium Deposition for Stable Anodes of Lithium-Metal Batteries. *J. Mater. Chem. A* **2019**, *7*, 2184−2191.

(9) Cong, Y.; Geng, Z.; Sun, Y.; Yuan, L.; Wang, X.; Zhang, X.; Wang, L.; Zhang, W.; Huang, K.; Feng, S. Cation Segregation of a-Site Deficiency Perovskite $La_{0.85}FeO_{3-\delta}$ Nanoparticles toward High-Performance Cathode Catalysts for Rechargeable Li-O_2 Battery. *ACS Appl. Mater. Interfaces* **2018**, *10*, 25465−25472.

(10) Shu, C.; Wu, C.; Long, J.; Guo, H.; Dou, S.-X.; Wang, J. Highly Reversible Li-O_2 Battery Induced by Modulating Local Electronic Structure via Synergistic Interfacial Interaction Between Ruthenium Nanoparticles and Hierarchically Porous Carbon. *Nano Energy* **2019**, *57*, 166−175.

(11) Yu, H.; Dinh, K. N.; Sun, Y.; Fan, H.; Wang, Y.; Jing, Y.; Li, S.; Srinivasan, M.; Yan, Q. Performance-Improved Li-O_2 Batteries by Tailoring the Phases of Mo_xC Porous Nanorods as an Efficient Cathode. *Nanoscale* **2018**, *10*, 14877−14884.
(12) Deng, H.; Qiao, Y.; Zhang, X.; Qiu, F.; Chang, Z.; He, P.; Zhou, H. Killing Two Birds with One Stone: a Cu Ion Redox Mediator for a Non-Aqueous Li-O_2 Battery. *J. Mater. Chem. A* **2019**, *7*, 17261−17265.
(13) Kim, H.; Kwak, W.-J.; Jung, H.-G.; Sun, Y.-K. Verification for Trihalide Ions as Redox Mediators in Li-O_2 Batteries. *Energy Storage Mater.* **2019**, *19*, 148−153.
(14) Dong, Q.; Yao, X.; Zhao, Y.; Qi, M.; Zhang, X.; Sun, H.; He, Y.; Wang, D. Cathodically Stable Li-O_2 Battery Operations Using Water-in-Salt Electrolyte. *Chem* **2018**, *4*, 1345−1358.
(15) Assary, R. S.; Lu, J.; Du, P.; Luo, X.; Zhang, X.; Ren, Y.; Curtiss, L. A.; Amine, K. The Effect of Oxygen Crossover on the Anode of a Li-O_2 Battery Using an Ether-Based Solvent: Insights from Experimental and Computational Studies. *ChemSusChem* **2013**, *6*, 51−55.
(16) Lin, D.; Liu, Y.; Cui, Y. Reviving the Lithium Metal Anode for High-Energy Batteries. *Nat. Nanotechnol.* **2017**, *12*, 194−206.
(17) Guo, Z.; Wang, F.; Li, Z.; Yang, Y.; Tamirat, A. G.; Qi, H.; Han, J.; Li, W.; Wang, L.; Feng, S. Lithiophilic Co/Co_4N Nanoparticles Embedded in Hollow N-Doped Carbon Nanocubes Stabilizing Lithium Metal Anodes for Li-Air Batteries. *J. Mater. Chem. A* **2018**, *6*, 22096−22105.
(18) Kim, B. G.; Kim, J.-S.; Min, J.; Lee, Y.-H.; Choi, J. H.; Jang, M. C.; Freunberger, S. A.; Choi, J. W. A Moisture- and Oxygen-Impermeable Separator for Aprotic Li-O_2 Batteries. *Adv. Funct. Mater.* **2016**, *26*, 1747−1756.
(19) Xin, X.; Ito, K.; Dutta, A.; Kubo, Y. Dendrite-Free Epitaxial Growth of Lithium Metal during Charging in Li-O_2 Batteries. *Angew. Chem., Int. Ed.* **2018**, *57*, 13206−13210.
(20) Song, H.; Deng, H.; Li, C.; Feng, N.; He, P.; Zhou, H. Advances in Lithium-Containing Anodes of Aprotic Li-O_2 Batteries: Challenges and Strategies for Improvements. *Small Methods* **2017**, *1*, 1700135.
(21) Zhang, P.; Zhao, Y.; Zhang, X. Functional and Stability Orientation Synthesis of Materials and Structures in Aprotic Li-O_2 Batteries. *Chem. Soc. Rev.* **2018**, *47*, 2921−3004.
(22) Yin, Y.-B.; Yang, X.-Y.; Chang, Z.-W.; Zhu, Y.-H.; Liu, T.; Yan, J.-M.; Jiang, Q. A Water-/Fireproof Flexible Lithium-Oxygen Battery Achieved by Synergy of Novel Architecture and Multifunctional Separator. *Adv. Mater.* **2018**, *30*, 1703791.
(23) Luo, K.; Zhu, G.; Zhao, Y.; Luo, Z.; Liu, X.; Zhang, K.; Li, Y.; Scott, K. Enhanced Cycling Stability of Li-O_2 Batteries by Using a Polyurethane/SiO_2/Glass Fiber Nanocomposite Separator. *J. Mater. Chem. A* **2018**, *6*, 7770−7776.
(24) Xu, J.-J.; Liu, Q.-C.; Yu, Y.; Wang, J.; Yan, J.-M.; Zhang, X.-B. In Situ Construction of Stable Tissue-Directed/Reinforced Bifunctional Separator/Protection Film on Lithium Anode for Lithium-Oxygen Batteries. *Adv. Mater.* **2017**, *29*, 1606552.
(25) Koch, S. L.; Morgan, B. J.; Passerini, S.; Teobaldi, G. Density Functional Theory Screening of Gas-Treatment Strategies for Stabilization of High Energy-Density Lithium Metal Anodes. *J. Power Sources* **2015**, *296*, 150−161.
(26) Liu, Q.-C.; Xu, J.-J.; Yuan, S.; Chang, Z.-W.; Xu, D.; Yin, Y.-B.; Li, L.; Zhong, H.-X.; Jiang, Y.-S.; Yan, J.-M.; Zhang, X.-B. Artificial Protection Film on Lithium Metal Anode toward Long-Cycle-Life Lithium-Oxygen Batteries. *Adv. Mater.* **2015**, *27*, 5241−5247.
(27) Yoo, E.; Zhou, H. Enhanced Cycle Stability of Rechargeable Li-O_2 Batteries by the Synergy Effect of a LiF Protective Layer on the Li and DMTFA Additive. *ACS Appl. Mater. Interfaces* **2017**, *9*, 21307−21313.
(28) Asadi, M.; Sayahpour, B.; Abbasi, P.; Ngo, A. T.; Karis, K.; Jokisaari, J. R.; Liu, C.; Narayanan, B.; Gerard, M.; Yasaei, P.; Hu, X.; Mukherjee, A.; Lau, K. C.; Assary, R. S.; Khalili-Araghi, F.; Klie, R. F.; Curtiss, L. A.; Salehi-Khojin, A. A Lithium-Oxygen Battery with a Long Cycle Life in an Air-Like Atmosphere. *Nature* **2018**, *555*, 502−506.
(29) Huang, Z.; Ren, J.; Zhang, W.; Xie, M.; Li, Y.; Sun, D.; Shen, Y.; Huang, Y. Protecting the Li-Metal Anode in a Li-O_2 Battery by Using Boric Acid as an SEI-Forming Additive. *Adv. Mater.* **2018**, *30*, 1803270.
(30) Tang, W.; Yin, X.; Chen, Z.; Fu, W.; Loh, K. P.; Zheng, G. W. Chemically Polished Lithium Metal Anode for High Energy Lithium Metal Batteries. *Energy Storage Mater.* **2018**, *14*, 289−296.
(31) Luo, Z.; Zhu, G.; Guo, L.; Li, F.; Li, Y.; Fu, M.; Cao, Y.-C.; Li, Y.-L.; Luo, K. Improving Cyclability and Capacity of Li-O_2 Batteries via Low Rate Pre-Activation. *Chem. Commun.* **2019**, *55*, 2094−2097.
(32) Sun, Z.; Wang, H.-R.; Wang, J.; Zhang, T. Oxygen-Free Cell Formation Process Obtaining LiF Protected Electrodes for Improved Stability in Lithium-Oxygen Batteries. *Energy Storage Mater.* **2019**, *23*, 670−677.
(33) Zhang, X.; Zhang, Q.; Wang, X.-G.; Wang, C.; Chen, Y.-N.; Xie, Z.; Zhou, Z. An Extremely Simple Method for Protecting Lithium Anodes in Li-O_2 Batteries. *Angew. Chem., Int. Ed.* **2018**, *57*, 12814−12818.
(34) Liao, K.; Wu, S.; Mu, X.; Lu, Q.; Han, M.; He, P.; Shao, Z.; Zhou, H. Developing a "Water-Defendable" and "Dendrite-Free" Lithium-Metal Anode Using a Simple and Promising $GeCl_4$ Pretreatment Method. *Adv. Mater.* **2018**, *30*, 1705711.
(35) Zhang, T.; Liao, K.; He, P.; Zhou, H. A Self-Defense Redox Mediator for Efficient Lithium-O_2 Batteries. *Energy Environ. Sci.* **2016**, *9*, 1024−1030.
(36) Zhao, X.; Sun, Z.; Yao, Z.; Cui, Z.; Wang, J.; Zhang, T. Halosilane Triggers Anodic Silanization and Cathodic Redox for Stable and Efficient Lithium-O_2 Batteries. *J. Mater. Chem. A* **2019**, *7*, 18237−18243.
(37) Lee, D. J.; Lee, H.; Song, J.; Ryou, M.-H.; Lee, Y. M.; Kim, H.-T.; Park, J.-K. Composite Protective Layer for Li Metal Anode in High-Performance Lithium-Oxygen Batteries. *Electrochem. Commun.* **2014**, *40*, 45−48.
(38) Kim, J.-H.; Woo, H.-S.; Kim, W. K.; Ryu, K. H.; Kim, D.-W. Improved Cycling Performance of Lithium-Oxygen Cells by use of a Lithium Electrode Protected with Conductive Polymer and Aluminum Fluoride. *ACS Appl. Mater. Interfaces* **2016**, *8*, 32300−32306.
(39) Li, N.; Zhang, K.; Xie, K.; Wei, W.; Gao, Y.; Bai, M.; Gao, Y.; Hou, Q.; Shen, C.; Xia, Z.; Wei, B. Reduced-Graphene-Oxide-Guided Directional Growth of Planar Lithium Layers. *Adv. Mater.* **2019**, *32*, 1907079.
(40) Kim, J.-S.; Kim, D. W.; Jung, H. T.; Choi, J. W. Controlled Lithium Dendrite Growth by a Synergistic Effect of Multilayered Graphene Coating and an Electrolyte Additive. *Chem. Mater.* **2015**, *27*, 2780−2787.
(41) Zhao, J.; Zhou, G.; Yan, K.; Xie, J.; Li, Y.; Liao, L.; Jin, Y.; Liu, K.; Hsu, P.-C.; Wang, J.; Cheng, H.-M.; Cui, Y. Air-Stable and Freestanding Lithium Alloy/Graphene Foil as an Alternative to Lithium Metal Anodes. *Nat. Nanotechnol.* **2017**, *12*, 993−999.
(42) Shen, X.; Li, Y.; Qian, T.; Liu, J.; Zhou, J.; Yan, C.; Goodenough, J. B. Lithium Anode Stable in Air for Low-Cost Fabrication of a Dendrite-Free Lithium Battery. *Nat. Commun.* **2019**, *10*, 900.
(43) Gao, Y.; Yan, Z.; Gray, J. L.; He, X.; Wang, D.; Chen, T.; Huang, Q.; Li, Y. C.; Wang, H.; Kim, S. H.; Mallouk, T. E.; Wang, D. Polymer-Inorganic Solid-Electrolyte Interphase for Stable Lithium Metal Batteries under Lean Electrolyte Conditions. *Nat. Mater.* **2019**, *18*, 384−389.
(44) Tang, S.; Lan, Q.; Xu, L.; Liang, J.; Lou, P.; Liu, C.; Mai, L.; Cao, Y.-C.; Cheng, S. A Novel Cross-Linked Nanocomposite Solid-State Electrolyte with Super Flexibility and Performance for Lithium Metal Battery. *Nano Energy* **2020**, *71*, 104600.
(45) Lin, D.; Yuen, P. Y.; Liu, Y.; Liu, W.; Liu, N.; Dauskardt, R. H.; Cui, Y. A Silica-Aerogel-Reinforced Composite Polymer Electrolyte with High Ionic Conductivity and High Modulus. *Adv. Mater.* **2018**, *30*, 1802661.
(46) Luo, Z.; Zhu, L.; Zhang, H.; Tang, H. Polyaniline Uniformly Coated on Graphene Oxide Sheets as Supercapacitor Material with Improved Capacitive Properties. *Mater. Chem. Phys.* **2013**, *139*, 572−579.
(47) Xu, J.; Wang, K.; Zu, S.-Z.; Han, B.-H.; Wei, Z. Hierarchical Nanocomposites of Polyaniline Nanowire Arrays on Graphene Oxide Sheets with Synergistic Effect for Energy Storage. *ACS Nano* **2010**, *4*, 5019−5026.

https://dx.doi.org/10.1021/acsami.0c08355
ACS Appl. Mater. Interfaces 2020, 12, 27316−27326

(48) Liu, S.; Deng, L.; Guo, W.; Zhang, C.; Liu, X.; Luo, J. Bulk Nanostructured Materials Design for Fracture-Resistant Lithium Metal Anodes. *Adv. Mater.* **2019**, *31*, 1807585.
(49) Cheng, X.-B.; Yan, C.; Peng, H.-J.; Huang, J.-Q.; Yang, S.-T.; Zhang, Q. Sulfurized Solid Electrolyte Interphases with a Rapid Li^+ Diffusion on Dendrite-Free Li Metal Anodes. *Energy Storage Mater.* **2018**, *10*, 199−205.
(50) Pan, R.; Sun, R.; Wang, Z.; Lindh, J.; Edström, K.; Strømme, M.; Nyholm, L. Sandwich-Structured Nano/Micro Fiber-Based Separators for Lithium Metal Batteries. *Nano Energy* **2019**, *55*, 316−326.
(51) Ye, H.; Zheng, Z. J.; Yao, H. R.; Liu, S. C.; Zuo, T. T.; Wu, X. W.; Yin, Y. X.; Li, N. W.; Gu, J. J.; Cao, F. F.; Guo, Y. G. Guiding Uniform Li Plating/Stripping via Lithium Aluminum Alloying Medium for Long-Life Li Metal Batteries. *Angew. Chem., Int. Ed.* **2019**, *58*, 1094−1099.
(52) Sun, F.; Gao, R.; Zhou, D.; Osenberg, M.; Dong, K.; Kardjilov, N.; Hilger, A.; Markötter, H.; Bieker, P. M.; Liu, X.; Manke, I. Revealing Hidden Facts of Li Anode in Cycled Lithium-Oxygen Batteries through X-Ray and Neutron Tomography. *ACS Energy Lett.* **2019**, *4*, 306−316.
(53) Bai, S.; Sun, Y.; Yi, J.; He, Y.; Qiao, Y.; Zhou, H. High-Power Li-Metal Anode Enabled by Metal-Organic Framework Modified Electrolyte. *Joule* **2018**, *2*, 2117−2132.
(54) Zhang, R.; Chen, X.; Shen, X.; Zhang, X.-Q.; Chen, X.-R.; Cheng, X.-B.; Yan, C.; Zhao, C.-Z.; Zhang, Q. Coralloid Carbon Fiber-Based Composite Lithium Anode for Robust Lithium Metal Batteries. *Joule* **2018**, *2*, 764−777.
(55) Zhang, H.; Liao, X.; Guan, Y.; Xiang, Y.; Li, M.; Zhang, W.; Zhu, X.; Ming, H.; Lu, L.; Qiu, J.; Huang, Y.; Cao, G.; Yang, Y.; Mai, L.; Zhao, Y.; Zhang, H. Lithiophilic-Lithiophobic Gradient Interfacial Layer for a Highly Stable Lithium Metal Anode. *Nat. Commun.* **2018**, *9*, 3729.
(56) Liu, Y.; Xiong, S.; Wang, J.; Jiao, X.; Li, S.; Zhang, C.; Song, Z.; Song, J. Dendrite-Free Lithium Metal Anode Enabled by Separator Engineering via Uniform Loading of Lithiophilic Nucleation Sites. *Energy Storage Mater.* **2019**, *19*, 24−30.
(57) Wang, X.; Wang, B.; Tang, Y.; Xu, B. B.; Liang, C.; Yan, M.; Jiang, Y. Manganese Hexacyanoferrate Reinforced by PEDOT Coating Towards High-rate and Long-life Sodium-ion Battery Cathode. *J. Mater. Chem. A* **2020**, *8*, 3222−3227.
(58) Kwak, W.-J.; Park, J.; Nguyen, T. T.; Kim, H.; Byon, H. R.; Jang, M.; Sun, Y.-K. A dendrite- and oxygen-proof protective layer for lithium metal in lithium-oxygen batteries. *J. Mater. Chem. A* **2019**, *7*, 3857−3862.

https://dx.doi.org/10.1021/acsami.0c08355
ACS Appl. Mater. Interfaces 2020, 12, 27316−27326